Robb, P., Finnie, M., Longo, P., and Craven, A. (2012) *Experimental evaluation of interfaces using atomic-resolution high angle annular dark field (HAADF) imaging*. Ultramicroscopy, 114. pp. 11-19. ISSN 0304-3991

http://eprints.gla.ac.uk/66668/

Deposited on: 29 June 2012

Enlighten – Research publications by members of the University of Glasgow
http://eprints.gla.ac.uk

Experimental evaluation of interfaces using atomic-resolution high angle annular dark field (HAADF) imaging

Paul D. Robb[1,2*], Michael Finnie[1], Paolo Longo[1], Alan J. Craven[1,2]

[1]Department of Physics & Astronomy, University of Glasgow, G12 8QQ, UK

[2]SuperSTEM Laboratory, Daresbury Laboratory, WA4 4AD, UK

**Correspondence:* Room 402
Department of Physics and Astronomy
University of Glasgow
Glasgow G12 8QQ
p.robb@physics.gla.ac.uk

Abstract

Aberration-corrected high angle annular dark field (HAADF) imaging in scanning transmission electron microscopy (STEM) can now be performed at atomic-resolution. This is an important tool for the characterisation of the latest semiconductor devices that require individual layers to be grown to an accuracy of a few atomic layers. However, the actual quantification of interfacial sharpness at the atomic-scale can be a complicated matter. For instance, it is not clear how the use of the total, atomic column or background HAADF signals can affect the measured sharpness or individual layer widths. Moreover, a reliable and consistent method of measurement is necessary. To highlight these issues, two types of AlAs / GaAs interfaces were studied in-depth by atomic-resolution HAADF imaging. A method of analysis was developed in order to map the various HAADF signals across an image and to reliably determine interfacial sharpness. The results demonstrated that the level of perceived interfacial sharpness can vary significantly with specimen thickness and the choice of HAADF signal. Individual layer widths were also shown to have some dependence on the choice of HAADF signal. Hence, it is crucial to have an awareness of which part of the HAADF signal is chosen for analysis along with possible specimen thickness effects for future HAADF studies performed at the scale of a few atomic layers.

Keywords: HAADF imaging; interfaces; image processing

1. Introduction

The sharpness of semiconductor layers is an active area of interest as the quality of such structures has a direct influence on the electronic and optical properties of the latest high-speed semiconductor devices [1-4]. In this context, interfacial sharpness is considered a general term for the level of deviation from a perfect interface that gives rise to a compositional transition region between two materials. Techniques, such as molecular beam epitaxy (MBE), are typically used to grow semiconductor layers with a quality of the order of a few atomic layers [5]. In order to investigate the interfacial sharpness of semiconductors (and other materials), high angle annular dark field (HAADF) imaging in scanning transmission electron microscopy (STEM) is frequently employed [6-9]. The underlying theory of HAADF imaging has been discussed by many authors [10-16]. In essence, this technique relies on the application of an annular detector with a large inner angle (>50mrad at 100kV accelerating voltage) in order to collect electrons that have undergone high angle elastic or thermal diffuse scattering. The collection of, in effect, Rutherford-like scattering results in the atomic number (Z) sensitivity that is typically associated with HAADF images [10-16]. In a simple qualitative model of image contrast, high-spatial resolution information in HAADF images is associated with atomic column intensities that sit on top of a background signal [17-19]. Whereas the column signals are related to the phenomenon of probe channelling (i.e. the tendency of the probe to remain on an atomic column for a certain depth), the background signal is generated from the average scattering from the material volume that is sampled by the de-channelled probe [20-21]. The background therefore gives non-local information about the specimen.

The ability of HAADF imaging to provide information at the atomic scale has been greatly improved through the recent development of aberration-corrected instruments [22-25]. For example, SuperSTEM 1 was the first UK based aberration-corrected 100kV FEG-STEM (field emission gun-STEM) that was capable of achieving a spatial resolution of 1Å. It is now a routine matter to obtain this level of resolution and the use of aberration-corrected microscopes is widespread. Hence, the availability of these instruments now provides the opportunity to investigate composition across semiconductor interfaces with the necessary sensitivity at the scale of individual atomic layers.

It is a straightforward exercise to interpret HAADF images of thin bulk materials (if the spacing of atomic columns is greater than the probe size) in terms of composition [17]. In this case, the underlying uniform background signal can be disregarded and the local composition can be estimated from the column signals. Other authors have also developed a method to quantify the total intensity of individual atomic columns using statistical parameter estimation theory in order to estimate their relative composition [26]. Nevertheless, an accurate evaluation of interface quality from atomic-resolution HAADF data is a complicated and problematical matter due to a number of factors. First of all, the reason behind any perceived non-sharpness can be difficult to ascertain as HAADF imaging presents a two dimensional projection through the entire thickness of a specimen that may have different sharpness profiles in three dimensions. As it is commonly recommended that analysis should be performed on very thin crystals, the interfacial profile is only investigated over small depths (~10nm). This means that a flawed assessment of an interface quality is likely to be made especially in cases where vicinal and stepped profiles are present. Hence, it is not certain if it is justified to estimate interfacial sharpness from a single image taken at a particular thickness.

Another issue concerns what criteria should actually be employed to measure interfacial sharpness from HAADF images. Without atomic-resolution imaging, the distance over which the change in the total HAADF signal occurs (across a boundary) is used as a measure of the interfacial sharpness [27-28]. In the case of atomic-resolution images, the change in the total, column and background signals can all be used to measure interfacial sharpness. However, it is not clear if the choice of signal has an effect on the level of sharpness that is measured. In practice, intensity line profiles are usually visually inspected in order to determine the distance over which the total or column signal changes and then this figure is quoted as a measure of the sharpness (typically in integral units of atomic layers). This can result in a subjective and inaccurate interpretation of the interface width. This problem is exacerbated when the background signal changes rapidly between layers of very different average atomic number and, thus, it is not straightforward to separate the column intensities from the background. Consequently, an intensity line profile taken across this type of region will be difficult to interpret in terms of atomic species. In addition, if the depth over which probe channelling occurs is markedly different down the various types of atomic columns then compositional changes may be detected at different depths in different columns across a

boundary. Furthermore, it is often the case that layers are not uniformly sharp in the $[1\bar{1}0]$ direction [27-28]. Therefore, it is not certain how to properly evaluate interfaces that have a range of sharpness values.

To highlight and address the issues outlined above, this paper presents an examination into the measurement of the sharpness of [110]-oriented AlAs / GaAs interfaces using atomic-resolution HAADF images taken from SuperSTEM 1. This system was chosen for study not only because (GaAl)As system is relevant for applications in high-mobility semiconductor devices but also because the order in which the materials are grown controls the sharpness of the resultant interface [30]. For instance, an interface made from AlAs grown on top of GaAs (termed an AlAs-on-GaAs interface) is generally rougher and less well defined than the opposite configuration with GaAs grown on AlAs (GaAs-on-AlAs interface) [1,28-30]. It is unclear whether this is a result of differing levels of elemental diffusion and / or stepping in each interface. Hence, the AlAs / GaAs system allows the effect of two different sharpness characteristics to be investigated and hence whether the differences between the interfaces can be detected and distinguished using HAADF imaging. To accomplish this, first a practical approach is presented for the quantification of the sharpness from the atomic resolution information available from the column intensities in a HAADF image. Interfacial sharpness and layer widths are then considered as a function of specimen thickness and a comparison is made with the results obtained by using the total, column and background signals. This leads to a number of implications for the quantification of atomic-scale materials using HAADF imaging.

2. Experimental

2.1 Sample preparation

Bulk AlAs, bulk GaAs and AlAs / GaAs interfaces were all grown epitaxially on the same GaAs wafer along the [001] crystal direction by MBE [1-3]. The substrate was polished to a tolerance of $\pm 0.5^{o}$. No wafer rotation was employed during the growth process and the materials were grown at a substrate temperature of 730°C.

AlAs / GaAs interfaces were investigated from isolated interfaces between wide layers (50nm) of AlAs and GaAs and from a superlattice made from 20 repeats of 9ML AlAs / 9ML

GaAs. 1ML (monolayer) is defined as containing 2 atomic planes in which one is composed of Group III atoms (either Al or Ga) and the other is composed of Group V atoms (always As in AlAs and GaAs). The Z numbers of Al, Ga and As are 13, 31 and 33, respectively. STEM samples were prepared using the conventional cross-section technique and were finished with a low energy ion mill at 400eV and at an angle of 6° using a Technoorg GentleMill [31]. The specimen was orientated along the [110] direction using the primary wafer flat as a reference. The projection along any <110> direction forms the familiar dumbbell configuration that is characteristic of zinc-blende materials [1-3]. In this way, every dumbbell (i.e. every monolayer) is constructed from a column of Group III atoms and a column of As atoms. These columns are separated by ~1.4Å in AlAs and GaAs. All of the analysis performed for this paper refers exclusively to specimens oriented in the [110] direction.

2.2 Data acquisition

All of the experimental results were obtained from a single session using SuperSTEM 1. This is a 100kV FEG-STEM that is equipped with a second generation NION aberration corrector [23-24]. The cold FEG of the microscope has a gun brightness of about $10^{9}Acm^{-2}Sr^{-1}$ and an energy spread of 0.3eV. A probe semi-convergence angle of 24mrad was employed and HAADF images were acquired using a scintillator-photomultiplier tube based detector whereas electron energy loss spectroscopy (EELS) data was collected with a Gatan-ENFINA spectrometer (energy resolution ~0.35eV). All HAADF images had a pixel dwell time of 19µsec, a pixel size of 0.0146nm and were composed of 1024 × 1024 pixels. In the mode of operation used, the HAADF detector has inner and outer angles of 70mrad and 210mrad, respectively. In addition, at the beginning of the experiment, the image intensity black level was set so that a few image counts (~5-10) were recorded in the absence of any specimen material above the noise. Typical image counts are of the order of several thousand in the presence of the specimen. Furthermore, a specimen drift rate of much less than 5nm per hour can be achieved in SuperSTEM 1.

Only images that demonstrated reflections out to a spatial resolution of 1Å (found from the Fourier transform of each image) and that were taken over a uniform and flat area of specimen were considered. After an image had been acquired, the probe was scanned rapidly across the entire image area and 50 low loss EELS spectra were averaged. The Digital Micrograph software package was then used to obtain a measure of the specimen thickness

for a particular image. Egerton describes the procedure of obtaining a material's mean free path and, subsequently, the absolute specimen thickness if the beam energy, STEM convergence semi-angle, EELS collection semi-angle and effective Z number of the material are known [32].

3. HAADF signal mapping

3.1 Dumbbell signals

Fig. 1(a) shows a HAADF image of an isolated AlAs-on-GaAs interface (at a specimen thickness of ~50nm) with the crystal structure partly overlaid. The upper plot in Fig. 1(b) provides an example of a typical HAADF intensity profile taken across such an interface. The profile was taken from the area indicated in Fig. 1(a). Every point of the intensity profile was generated from the average of 20 image pixels summed along the entire $[1\bar{1}0]$ direction of the image area (the image in Fig. 1(a) illustrates the crystal directions). The quality of an interface is usually estimated from the inspection of such profiles. It is clear from Fig. 1(b) that not only does the total intensity drop from GaAs to AlAs but that the shape of the individual dumbbells also changes to become more asymmetric in AlAs. To a first approximation, the change in the total intensity is related to the higher background signal generated by the high Z GaAs compared to AlAs. On the other hand, the shape of each dumbbell is associated with the respective Group III and Group V (always As) column signals. The lower plot in Fig. 1(b) provides the intensity profile of the column signals without the background. The removal of the background is described in Section 3.3. Fig. 1(b) also highlights an interfacial region in which one dumbbell shape is intermediate between that of GaAs and AlAs. The labelled dumbbell in Fig. 1(b) demonstrates four important measurements which are sufficient to evaluate the various signals of a particular dumbbell. These are the total HAADF signal at the Group III column (I_{III}), at the Group V column (I_V) and the background signals under both columns of the dumbbell in question (I_{BIII} and I_{BV}). The extraction of these values for each dumbbell in an image allows the behaviour of the different signals to be ascertained.

A useful way to quantify the shape of a dumbbell is to calculate the column ratio [33]. This is defined as $(I_{III} - I_{BIII}) / (I_V - I_{BV})$ and provides an estimate of the average scattering strength of the channelled region of the Group III column relative to that of the neighbouring Group V

column. Since As is the only Group V element present across AlAs / GaAs interfaces, the change in the intended composition (due to roughness) is manifested only in the composition of the Group III column of interfacial dumbbells. Nevertheless, localised differences in specimen preparation damage, point defects and contamination can slightly affect the HAADF signal of individual Group III and Group V columns across a region of uniform thickness. Hence, to compare individual Group III columns across an image, the column ratio uses each neighbouring As column signal as a reference point thereby minimising the effect of localised differences in specimen quality. At sufficiently low thicknesses, high Z Group III columns will give a large value of the column ratio compared to low Z Group III columns.

The processing technique of column ratio mapping was developed in order to convert a HAADF image into a map that shows the column ratio value of every dumbbell present, thereby allowing the local composition to be estimated at a glance [33]. In a similar way, maps of the total, column and background signals can also be produced. The analysis of all experimental data presented in this paper is based on the extraction of the various signals and the generation of the respective maps. For brevity, the method of analysis for a single image is provided mainly in terms of the column ratio but also applies for the other signals. A comparison of interfacial sharpness measured using the column ratio, Group III total, Group III column and background signals is given at the end. In addition, the change in the measured semiconductor layer width using the Group III column and background signals is also provided.

3.2 Extraction of total and background signals

An automated procedure is used to accurately extract the total and background signals of every individual dumbbell in an image. The column signals are extracted in a slightly different way as described below. An automated procedure is necessary as a typical HAADF image can sometimes contain several thousand dumbbells. Given the location of one dumbbell in an image of the same structure and orientation, the approximate position of adjacent dumbbells can be established through the use of translation vectors. The average translation vector has an appropriate value in order to shift from the centre of one dumbbell to the next one in the same row. However, a HAADF image is often distorted by scan noise, scan coil hysteresis and changes in magnification across the image. Hence, a Matlab script

was developed to employ a form of pattern matching in order to locate the atomic columns accurately [34].

In the first step of the script operation, the image is rotated to vertically align any interface that is present. The growth direction ([001]) is always aligned left to right. An image section that is free from obvious image artefacts is then selected and used to define the total number of horizontal and vertical dumbbell rows to be processed. Fig. 2(a) shows an area of an image that was rotated and ready to be processed. An image sub-section is then identified around the current dumbbell to be processed (Fig. 2(b)). The dumbbell sub-section is then overlaid and compared to a reference area through the use of a cross-correlation function. The reference area consists of Gaussians that describe the expected size, shape and separation of the total column intensities (Fig. 2(c)). The form of the Gaussians can be varied using two parameters called the peak separation and the vertical skew (see Fig. 2(c)). The optimum parameter values are those that generate the maximum correlation coefficient. In this way, the location of the total column intensities can be established for each dumbbell sub-section. The values of I_{III} and I_V are then measured by integrating over 3×3 pixels to reduce the effect of noise. These 3×3 pixel windows are shown in Fig. 2(d). A similar method using inverted Gaussians is used to measure the minimum background positions around each dumbbell. The same process is performed for every dumbbell (and background position) in the image through the use of translation vectors to move from one dumbbell to the next (Fig. 2(a)).

3.3 Extraction of column signals

The actual background signal under the Group III and V columns of a particular dumbbell, I_{BIII} and I_{BV}, must be removed in order to extract the respective column signals. This can be achieved by a combination of frequency filtering and interpolation as described in [33]. An interpolation using the 4 background signals (measured half way between the 4 nearest dumbbells in the horizontal and vertical directions) that surround each dumbbell is not used as small errors can arise in the interpolated background under the columns. The frequency filtering technique relies on the fact that the Fourier transform (FT) of a high-resolution HAADF image contains high frequency lattice reflections and a low frequency background modulation. The background modulation can be removed through the use of a low frequency mask (smoothed over 5 pixels) followed by an inverse FT that produces a background-subtracted image. Since the central scaling pixel of the FT is also removed by this method, it is

necessary to add an appropriate constant to the background-subtracted image to avoid negative intensity values. The same automated procedure described above is used on the background-removed image to measure the column signals from every dumbbell. However, the frequency filtering method often leaves a small residual intensity level due to the contribution of higher Fourier components to the background in some localised areas. Hence, an interpolated linear function is also employed to measure the residual background underneath both columns in every dumbbell in the background-subtracted image. The interpolated function uses the minimum intensity values (averaged over 3×3 pixels) on either side of the particular dumbbell as two end points (positions a and b in Fig. 1(b)). It should be noted that it is not clear if the real background under a dumbbell is significantly different to that between dumbbells as there is a possibility that the real background is reduced at column positions [35-36]. However, for the purposes of experimental measurement it is generally accepted to be the same. The background and column signals have been considered by other authors [13, 17, 20-21].

3.4 Signal Mapping

Maps that illustrate the behaviour of the various signals can be generated once the automated procedure is complete. For example, the integrated signal intensities at each atomic column can be used to calculate the column ratio for each processed dumbbell. The standard error in a single measurement of the column ratio is usually in the order of 1-2% (calculated from the standard deviation of the values in the 3×3 pixel windows). A standard HAADF image can then be converted into a map of the column ratio in which the relative positions of the dumbbells are replicated in a chess-board distribution along the [001] (x) and $[1\bar{1}0]$ (y) directions. An example of a column ratio map of the 9ML AlAs / 9ML GaAs superlattice (at a specimen thickness of ~30nm) can be seen in Fig. 3. The repeating layered structure is clearly evident in this case. In contrast to a standard HAADF image, the column ratio map highlights the distribution of local composition as it was generated from the high-spatial information of the column intensities. The column ratio values range from 0.21 to 1.27 in the map and the brightest dumbbells are most GaAs-like and the darkest dumbbells are most AlAs-like. The column ratio mean value of the AlAs (M_{AlAs}) and GaAs (M_{GaAs}) layers is equal to 0.41 and 0.97, respectively. The column ratio standard deviation of the AlAs (σ_{AlAs}) and GaAs (σ_{GaAs}) layers is equal to 0.094 and 0.085, respectively.

It is apparent that analysis conducted using column ratio mapping is not limited by problems of a modulated background at interfaces or by a subjective interpretation of dumbbell shapes as it uses an automated approach to measure column intensities. Furthermore, the technique gives a much better overall view of interfacial sharpness across the entire image compared to the standard method of analysis. For instance, the selected dumbbells along the central two interfaces in Fig. 3 (denoted by circles) have column ratio values in the range $M_{AlAs} + 2\sigma_{AlAs}$ to $M_{GaAs} - 2\sigma_{GaAs}$ i.e. 0.598 to 0.800. Since these dumbbells are intermediate between that of AlAs and GaAs (and outside two standard deviations of the appropriate mean values) they can be considered to be interfacial dumbbells. It can be seen that each interface does not have a consistent level of sharpness with some areas being atomically abrupt whilst others have a roughness over several monolayers. Hence, it is not adequate to evaluate interfacial sharpness from a few selected image regions due to the variation that is present.

4. Evaluation methods

4.1 Interface width

Fig. 4 provides a profile of the column ratio averaged over the entire y direction in Fig. 3. The error bars are equal to two times the standard error. In order to quantify the sharpness of the highlighted GaAs-on-AlAs interface, an error function was fitted to the column ratio profile. The error function was chosen as it has a similar profile to the column ratio profiles. It has three parameters that relate to the amplitude, width and lateral position. These parameters can be manipulated to accurately fit the function to any column ratio profile through a non-linear least-squares fitting procedure. The same function was also used for analysing profiles of the total, column and background signals. All fitting procedures were accomplished through the use of the Matlab Curve Fitting Toolbox [34]. The fitted error function can be seen in Fig. 4. The inflection point of the error function gives the mid-point of the interfacial region and its width provides one measure of the interfacial sharpness. In this case, the width is defined as the distance between the two points in the function that have values of 5% and 95%, respectively, of the full range of the fitted function. It should be noted that the fitted function will give a non-zero value for an ideally sharp interface. The sharpness of the GaAs-on-AlAs interface in Fig. 4 has a value of 3.23 ± 0.14ML using this measure. The error on the interfacial sharpness is calculated from the goodness of fit value given by Matlab. For comparison, Fig. 4(b) shows the fitting of the error function on the AlAs-on-GaAs interface.

In order to ascertain the range of sharpness values associated with each type of interface present in Fig. 3, the column ratio profile of every independent interleaved horizontal row of dumbbells was analysed in the manner described above. A typical column ratio map consists of 50 interleaving horizontal rows which are usually 40 dumbbells wide. The histogram of interface widths of the GaAs-on-AlAs interfaces is shown in Fig. 5. The existence of a range of sharpness values is dependent on the exact distribution of any steps and / or diffusion that are present at a particular location. Nevertheless, a particular interface can be characterised by considering its mean sharpness value. In the case of the GaAs-on-AlAs interface, its mean interface width is 3.27 ± 0.20ML. The error is equal to two times the standard error. Analysis conducted in this way allows the overall quality of interfaces to be evaluated whilst having an awareness of the variability present. Hence, it is clear that the fit of an error function to column ratio profiles provides a systematic and precise method of measuring interfacial sharpness and also gives an estimate of the error in the measurement. Equivalent analysis using the total, column and background signals can also be performed but is not provided here to avoid repetition. However, interfacial sharpness measured using the column ratio, Group III total, Group III column and background signals is considered in Section 5 along with the measured layer width using the Group III column and background signals.

4.2 Interface width as a function of specimen thickness

As was shown above, an atomic-resolution HAADF image of an AlAs / GaAs interface can be converted into a column ratio map that permits the sharpness at each point of the interface to be evaluated. This type of analysis was performed for the 9ML AlAs / GaAs superlattice and the isolated interfaces over a range of specimen thicknesses. For each thickness, a histogram of the interface width values was generated (similar to that in Fig. 5) and an average value was computed. The average interface width value (open circle) and the associated distribution (greyscale vertical stripe) are plotted, as a function of thickness, for AlAs-on-GaAs and GaAs-on-AlAs interfaces in Fig. 6(a) and Fig. 6(b), respectively. The greyscale bar at the right of each plot indicates the number of counts that contribute to each distribution.

Fig. 6(b) demonstrates that the average interface width of the GaAs-on-AlAs interface does not change significantly with specimen thickness. It can be seen that this type of interface has an average sharpness value equal to about 3ML over the thickness range considered. In

addition, at each thickness, there is a spread of interface values as demonstrated by the distribution stripes. Thus, the usual constraint of only analysing thin specimens may be relaxed in this case as the measured sharpness does not depend on the thickness of the specimen. However, in contrast to the GaAs-on-AlAs interface, Fig. 6(a) reveals that the sharpness of the AlAs-on-GaAs interface does vary with thickness. In this case, the interface width increases from about 3ML at a thickness of ~30nm up to about 6ML at a depth of ~90nm. Consequently, it is not always sufficient to gauge the growth quality from a single image of an interface.

4.3 Sharpness in the $[1\bar{1}0]$ direction

The measurement of the interface width outlined above masks any local roughness in the $[1\bar{1}0]$ direction along the interface. For example, an interface may be atomically abrupt along the growth direction even though the transition from one material to the next may be displaced in the $[1\bar{1}0]$ direction along each horizontal row. Hence, it is also important to consider how the position of the layers along an interface varies in the $[1\bar{1}0]$ direction.

Fig. 7(a) shows a column ratio map of the 9ML AlAs / 9ML GaAs superlattice (at a specimen thickness of ~55nm) with a selected 18ML wide region across the right hand side AlAs-on-GaAs interface (highlighted by the white box). The average column ratio profile across this region was measured and then fitted individually to each dumbbell row line trace in the selected region. This demonstrates how each row varies in comparison to the overall profile. Each fit of the average profile was performed through the use of a least-squares fitting method. In essence, the location of the best fit allows the position of each layer to be determined along a particular row of dumbbells. In the case of the GaAs layer in Fig. 7(a), the last dumbbell that is consistent with bulk GaAs (along a particular horizontal row) is represented by a small circle. The distribution of these GaAs layer end points was then plotted in the form of a histogram and a Gaussian fitted (see Fig. 7(b)). The FWHM (full width at half maximum) of the Gaussian was then used as a measure of the sharpness of the interface in the $[1\bar{1}0]$ direction. For the GaAs layer in Fig. 7(b), the width has a value of 1.93ML and indicates that the interface has a non-zero variation along the $[1\bar{1}0]$ direction. Similar analysis can be performed using the total, column and background signals once again.

It is apparent from Section 4.2 that to quote a single figure of sharpness for interfaces can lead to a flawed evaluation of their quality especially for interfaces that exhibit similar characteristics to the AlAs-on-GaAs interface. In fact, it is not clear how to adequately appraise such interfaces as their perceived sharpness varies significantly with specimen thickness. One way to gauge the relative quality of, for example, AlAs-on-GaAs and GaAs-on-AlAs interfaces is to compare their sharpness in the $[1\bar{1}0]$ direction. This gives an indication of their relative quality that is independent of the interface width along the growth direction. Fig. 8 shows how the $[1\bar{1}0]$ sharpness varies as a function of thickness for AlAs-on-GaAs and GaAs-on-AlAs interfaces. Only the data from the superlattice was considered as both types of interface can be analysed and compared at precisely the same thickness. Fig. 8 demonstrates that the AlAs-on-GaAs interface is in general rougher than the GaAs-on-AlAs interface in the $[1\bar{1}0]$ direction at most specimen thicknesses. However, there is no obvious trend in the measured roughness and the plots do not appear to depend on specimen thickness in any consistent manner.

5. Results and discussion

5.1 Interface width using different HAADF signals

Fig. 9(a) and Fig. 9(b) present a comparison of the average AlAs-on-GaAs and GaAs-on-AlAs, respectively, interface width using different signals extracted from HAADF images of the 9ML AlAs / 9ML GaAs superlattice as a function of thickness. The signals used are the column ratio (○), Group III total (■), Group III column (▲) and background signals (×). The Group V signal is not considered as only Group III columns are affected by interface roughness and the As column signal remains virtually constant across the image. The plots were generated using the technique outlined in Section 4.1 and Section 4.2.

From Fig. 9(a) it is apparent that the interface width measured using the column ratio, Group III total and Group III column signals all increase as the thickness is increased. The Group III total and Group III column signal plots also appear to have a similar gradient whereas the column ratio plot has a higher gradient. Moreover, the Group III total signal gives a wider measure of the AlAs-on-GaAs interface width than the Group III column signal. This behaviour is also observed for the GaAs-on-AlAs superlattice interface shown in Fig. 9(b) and is likely a result of the fact that the Group III total signal is partly made up of the

background signal that produces an additional widening of the interfaces. For instance, Fig. 9(a) and Fig. 9(b) demonstrate that the background signal plots stay fairly constant with thickness but have interface width values that are generally greater than those of the Group III column signal plots. Hence, the addition of the background to the Group III total signal results in a wider measure of interface width compared to that measured using only the Group III column signal. Furthermore, the reason that the background signal measured width does not change with thickness is possibly due to the superlattice layers not being wide enough to stop the background profiles of neighbouring layers from overlapping.

5.2 Layer width

For a complete characterisation of the latest semiconductor devices, it is crucial that the width of individual layers be determined. The width of a particular layer can be found from the separation of the mid-points of the interfacial regions on either side of the layer. The inflection point of the fitted error function was used to determine the interfacial mid-point. The error function was fitted to the profiles of the extracted HAADF signals as before and the average layer width of the AlAs and GaAs layers in the superlattice were computed. Fig. 10 shows how the AlAs and GaAs layer widths change with thickness using the Group III column and background signals. The column ratio and Group III total signal plots are similar in behaviour to the Group III column plot but are not shown for clarity.

It is interesting to note that the measured width of the nominally 9ML wide GaAs layer increases slightly with thickness using the Group III column signal. This is because, as the AlAs-on-GaAs interface widens with thickness, the Group III column intensity of last AlAs-like dumbbell saturates to become more GaAs-like and the interfacial mid-point moves progressively more into the AlAs region. On the other side of the GaAs layer, the interfacial mid-point does not change because the width of the GaAs-on-AlAs interface stays constant with thickness. Hence, the corresponding width of the AlAs layer reduces to keep the average width of the AlAs / GaAs pair constant, as required by the periodicity of the superlattice. The AlAs / GaAs pair has an average width equal to 8.51ML, which is less than the nominal figure of 9ML. Furthermore, if the plots were interpolated back to zero thickness then the AlAs and GaAs layers would have widths of 8.58ML and 8.54ML, respectively. In comparison, the width of the AlAs and GaAs layers do not change with thickness using the background signal. However, the GaAs layer is again generally wider than the AlAs layer and

the AlAs / GaAs pair has an average width equal to 8.6ML. These results suggest that the atomic-scale measurement of layer widths can also depend on which part of the HAADF signal is chosen for analysis along with the value of specimen thickness.

5.3 Implications for future experiments

It is clear that the perceived quality of some types of interface can be strongly dependent on the thickness of the specimen when HAADF imaging is used. Hence, the usual recommendation of analysing very thin specimens may lead to a flawed depiction of the interface under study. This is likely to be the case for stepped and vicinal interfaces in which the projected composition can change with depth. This has consequences for experiments that attempt to accurately compare the quality of, for example, the same interface grown under different conditions. Such experiments should at least be conducted at the same specimen thickness. In fact, the effect of specimen thickness should always be considered in experiments that attempt to measure the quality of interfaces to the accuracy of a few monolayers.

The actual part of the HAADF signal chosen for analysis can also have a significant impact on the observed sharpness. For instance, interfaces are perceived to be wider when the total HAADF signal is used in contrast to the use of the column signal over all thicknesses. When the background signal is used (at least for multilayer systems where the repeat length is small enough) no discernable change in interface width is observed as a function of thickness. Nonetheless, the background signal generally gives a wider estimate of interface sharpness at small thicknesses compared to the total and column signals. The choice of HAADF signal is also a relevant issue for the measurement of individual layer widths at the atomic-scale. For instance, the same layer can appear to have a different width when a different HAADF signal is used for analysis. If the column ratio, column or total signals are used then the perceived width of individual layers can also change as a function of specimen thickness. In the case of repeating multilayer structures, the average width of the repeating unit or the interpolated width at zero thickness can be used as an estimate of the ‘true’ layer widths. Hence, future HAADF experiments should have an awareness of how the choice of HAADF signal influences the measured attributes of a specimen especially if atomic-scale accuracy is required.

Fig. 9(a) and Fig. 9(b) suggest that the difference in the sharpness characteristics of the two types of interface can be distinguished by HAADF imaging if the analysis is performed over a range of thickness values using the column ratio, total signal or column signal. However, the reason(s) behind the changes in the interface widths measured by HAADF imaging at significant depths of crystal is difficult to ascertain. For instance, in order for the behaviour to be a consequence of local compositional changes at large thicknesses, a portion of the probe must remain channelled on some atomic columns to large depths. Although it is expected that the projected atomic potentials of relatively high Z (e.g. Ga and As) columns are strong enough to scatter away most of the probe intensity in the top portion of the crystal, the low Z (e.g. Al) columns may retain intensity to much greater depths. This may allow changes in local composition to influence the value of the column ratio or total / column signal at large thicknesses. However, another possibility is that the channelling does only occur in the top part of the specimen and the intensity that was scattered to high angles from this region is subsequently re-scattered due to the large thickness of the specimen. The measured column ratio or signal value would then vary at large depths without the probe being channelled. Hence, it cannot be stated for certain that the asymmetry in the results obtained for the two types of interface are a direct consequence of the differences in their growth quality. In order to aid the interpretation of the results, a series of simulated interfacial models will be considered in a future publication. Nonetheless, it is still evident that specimen thickness and the choice of HAADF signal can have a significant impact on atomic-scale measurements conducted through HAADF imaging.

6. Conclusions

The evaluation of interfacial sharpness through the use of atomic-resolution HAADF imaging requires a detailed and systematic approach. First of all, a HAADF image can be processed to separate out the various signals that contribute to the image. These include the total and column signals at atomic positions as well as the underlying background that provides only non-local information about the specimen. Once the signals have been extracted, they can be displayed in maps from which subsequent analysis can be performed. In the case of the AlAs-on-GaAs interface, the sharpness (measured by the column ratio, total and column signals) is strongly dependent on the specimen thickness. On the other hand, knowledge of the specimen thickness is not as important for the study of the GaAs-on-AlAs interface as the sharpness does not change with thickness. The actual part of the HAADF signal chosen to analyse

interfaces can also have an impact on the observed sharpness. For instance, the interfaces were always perceived to be wider when the total signal was used in contrast to the use of the column signal. When the background signal was used then no discernable change in interface width was observed. Layer widths were also found to be influenced by the choice of HAADF signal and specimen thickness. Hence, consideration should be given to which part of the HAADF signal is analysed as well as specimen thickness for future studies conducted at the atomic-scale.

Acknowledgements

This work was funded by the Engineering and Physical Sciences Research Council under grants GR/S41036/01 and EP/F002610/1 with support for one of the authors (MF) from the Doctoral Training Account. We are grateful to Martin Holland for growing the MBE materials and to Brian Miller for specimen preparation. We would also like to thank Andrew Bleloch, Mhairi Gass, Uwe Falke and Meiken Falke for SuperSTEM technical support and advice.

Figure captions

Fig. 1. (a) HAADF image of an isolated AlAs-on-GaAs interface at a specimen thickness of ~50nm with the crystal structure partially overlaid. (b) The upper plot shows an intensity profile taken from the box in (a). The lower plot in (b) gives the background-removed intensity profile.

Fig. 2. (a) Area of an image ready to be processed. (b) Current dumbbell sub-section to be processed. (c) Reference area with variable Gaussian shapes. (d) Final 3×3 pixel windows around the located Group III and V columns.

Fig. 3. Example of a column ratio map of the 9ML AlAs / 9ML GaAs superlattice at a specimen thickness of ~30nm. The circles highlight dumbbells with a value in the range 0.598 to 0.800 for the central GaAs-on-AlAs and AlAs-on-GaAs interfaces.

Fig. 4. (a) Column ratio profile averaged over the entire column ratio map in Fig. 3. An error function was fitted to the selected GaAs-on-AlAs interface. The interface width was

measured to be equal to 3.23 ± 0.21ML from the 5% and 95% limits of the error function. (b) The error function fitted to the neighbouring AlAs-on-GaAs interface.

Fig. 5. Histogram of interface widths measured from the column ratio map in Fig. 3 for GaAs-on-AlAs interfaces. The mean, standard deviation and standard error are also given.

Fig. 6. The variation of interface width as a function of specimen thickness for (a) AlAs-on-GaAs and (b) GaAs-on-AlAs interfaces using the column ratio. For each thickness, the distribution of width values is represented by the greyscale-coded vertical stripes. Also shown are the average interface width values (open circles).

Fig. 7. (a) Column ratio map of the 9ML AlAs / 9ML GaAs superlattice at a specimen thickness of ~55nm. An 18ML wide region around a AlAs-on-GaAs interface is highlighted (box). The position of the last GaAs-like dumbbell along each horizontal row is denoted by a small circle. (b) Histogram of the last GaAs-like dumbbell positions highlighted in (a). The FWHM of the fitted Gaussian gives a measure of the sharpness in the $[1\bar{1}0]$ direction.

Fig. 8. The variation of the width in the $[1\bar{1}0]$ direction as a function of specimen thickness for AlAs-on-GaAs and GaAs-on-AlAs interfaces. Only data from the 9ML AlAs / 9ML GaAs superlattice is shown.

Fig. 9. The variation of interface width as a function of specimen thickness for (a) AlAs-on-GaAs and (b) GaAs-on-AlAs superlattice interfaces using the column ratio, Group III total, Group III column and background signals.

Fig. 10. The variation of layer width as a function of specimen thickness for AlAs and GaAs layers in the superlattice. The Group III column and background signals were used to measure the layer widths.

Reference

[1] J. H. Davies, The physics of low-dimensional semiconductors, Cambridge University Press (2005)

[2] R. Enderlein, N. J. M. Horing, World Scientific (1999)

[3] S. M. Sze, Semiconductor devices: physics and technology, John Wiley & Sons, INC. (2002)

[4] D. O. Klenov, J. M. Zide, J. D. Zimmerman, A. C. Gossard, and S. Stemmer, Applied Physics Letters 86 (2005) 241901

[5] K. Y. Cheng, Proceedings of the IEEE, Vol. 85 (1997) No. 11

[6] S. C. Anderson, C. R. Birkeland, G. R. Anstis, D. J. H. Cockayne, Ultramicroscopy 69 (1997) 83-103

[7] T. Noda, N. Sumida, S. Koshiba, S. Nishioka, Y. Negi, E. Okunishi, Y. Akiyama, H. Sakaki, Journal of Crystal Growth 278 (2005) 569–574

[8] W. Neumann, Materials Chemistry and Physics 81 (2003) 364–367

[9] M. Valera, A. R. Lupini, K. van Benthem, A. Y. Borisevich, M. F. Chisholm, N. Shibata, E. Abe, S. J. Pennycook, Annual Review of Materials Research, Vol. 35 (2005) 359-569

[10] S. J. Pennycook, D. E. Jesson, Physical Review Letters, 64 (1990) 938-941

[11] S. J. Pennycook, D. E. Jesson, Ultramicroscopy 37, (1991) 14-38

[12] S. J. Pennycook, B. Rafferty, P. D. Nellist, Microscopy Microanalysis 6 (2000) 343-352

[13] C. Dwyer, J. Etheridge, Ultramicroscopy 96 (2003) 343-360

[14] R. F. Loane, P. Xu, J. Silcox, Ultramicroscopy 40 (1992) 121-138

[15] S. Hillyard, J. Silcox, Ultramicroscopy 58 (1995) 6-17

[16] B. Rafferty, P. Nellist, J. Pennycook, Journal of Electron Microscopy 50 (2001) 227-233

[17] D. O. Klenov, S. Stemmer, Ultramicroscopy 106 (2006) 889-901

[18] S. Van Aert, P. Geuens, D. van Dyck, C. Kisielowski, J. R. Jinschek, Ultramicroscopy 107 (2007) 551-558

[19] T. Plamann, M. J. Hytch, Ultramicroscopy 78 (1999) 153-161

[20] Y. Kotaka, Ultramicroscopy 110 (2010) 555–562

[21] M. Haruta, H. Kurata, H. Komatsu, Y. Shimakawa, S. Isoda, Ultramicroscopy 109 (2009) 361–367

[22] M. Haider, H. Rose, S. Uhlemann, E. Schwan, B. Kabius, K. Urban, Ultramicroscopy 75 (1998) 53-60

[23] N. Dellby, O L. Krivanek, P. D. Nellist, P. E. Batson, A. R. Lupini, Journal of Microscopy 50(3) (2001) 177-185

[24] O. L. Krivanek, N. Dellby, A. R. Lupini, Ultramicroscopy 78 (1999) 1-11

[25] O. L. Krivanek, P. D. Nellist, N. Dellby, M. F. Murfitt, Z. Szilagyi, Ultramicroscopy 96 (2003) 229-237

[26] S. Van Aert, J. Verbeeck, R. Erni, S. Bals, M. Luysberg, D. Van Dyck, G. Van Tendeloo, Ultramicroscopy 109 (2009) 1236–1244

[27] H. Larkner, B. Bollig, S. Ungerechts, E. Kubalek, Journal of Physics D: Applied Physics 29 (1996) 1767-1778

[28] N. Ikarashi, K. Ishida, Journal of Materials Science: Materials in Electronics 7 (1996) 285-295

[29] N. Ikarashi, T. Baba, K. Lshida, Applied Physics Letters 62 (1993) 1632-1634

[30] J. M. Moison, C. Guille, F. Houzay, F. Barthe, M. Van Rompay, Physical Review B Volume 40 9 (1989) 6149-6162

[31] C. P. Scott, A. J. Craven, P. Hatto, C. Davies, Journal of Microscopy, Vol. 182 Pt 3 (1996) pp. 186-191

[32] R. F. Egerton, Electron energy-loss spectroscopy in the electron microscope, 2nd edition, Plenum Press (1996)

[33] P. D. Robb and A. J. Craven, Ultramicroscopy, 109 (2008) 61-69

[34] www.mathworks.com, (2010)

[35] J. M. LeBeau, S. D. Findlay, X. Wang, A J. Jacobson, L. J. Allen, S. Stemmer, Physics Review. B 79 (2009) 214110

[36] C. B. Boothroyd, Journal of Microscopy 190 (1998) 99-108

Figures

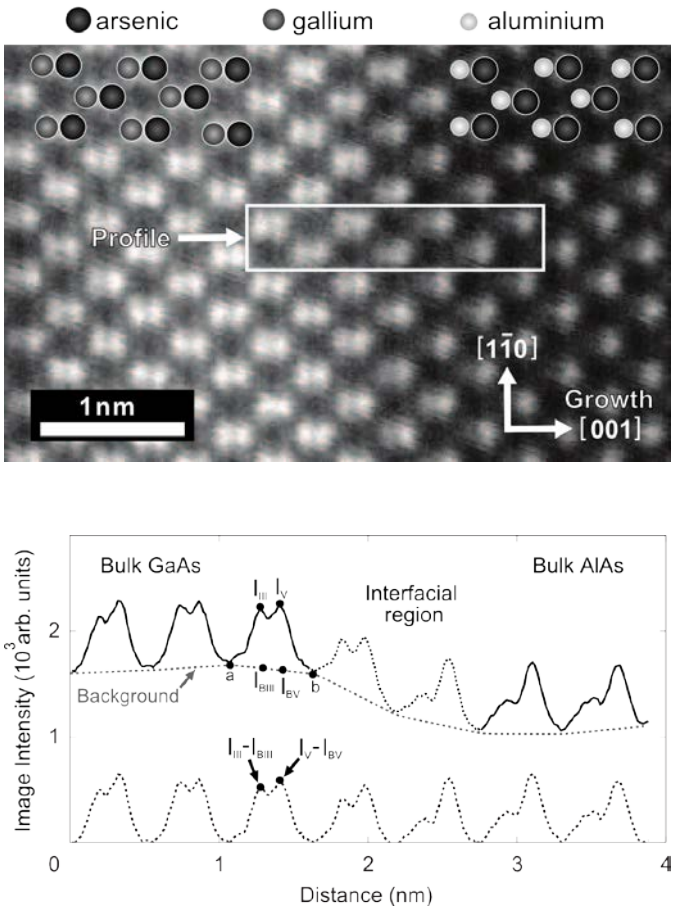

Fig. 1. (a) HAADF image of an isolated AlAs-on-GaAs interface at a specimen thickness of ~50nm with the crystal structure partially overlaid. (b) The upper plot shows an intensity profile taken from the box in (a). The lower plot in (b) gives the background-removed intensity profile.

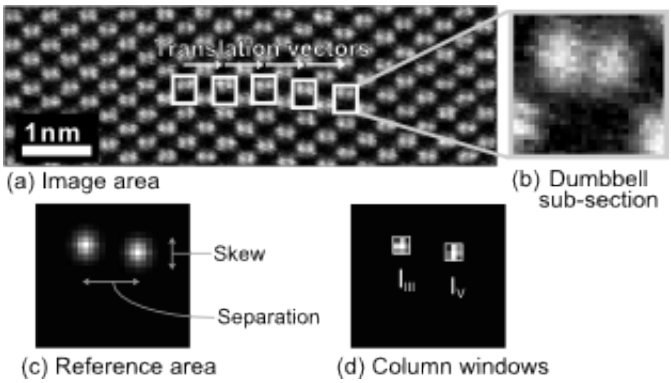

Fig. 2. (a) Area of an image ready to be processed. (b) Current dumbbell sub-section to be processed. (c) Reference area with variable Gaussian shapes. (d) Final 3×3 pixel windows around the located Group III and V columns.

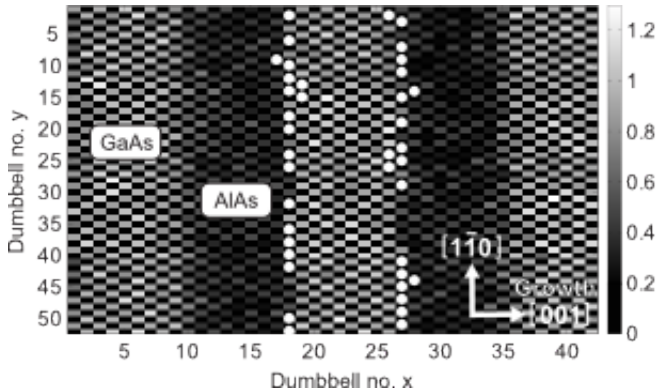

Fig. 3. Example of a column ratio map of the 9ML AlAs / 9ML GaAs superlattice at a specimen thickness of ~30nm. The circles highlight dumbbells with a value in the range 0.598 to 0.800 for the central GaAs-on-AlAs and AlAs-on-GaAs interfaces.

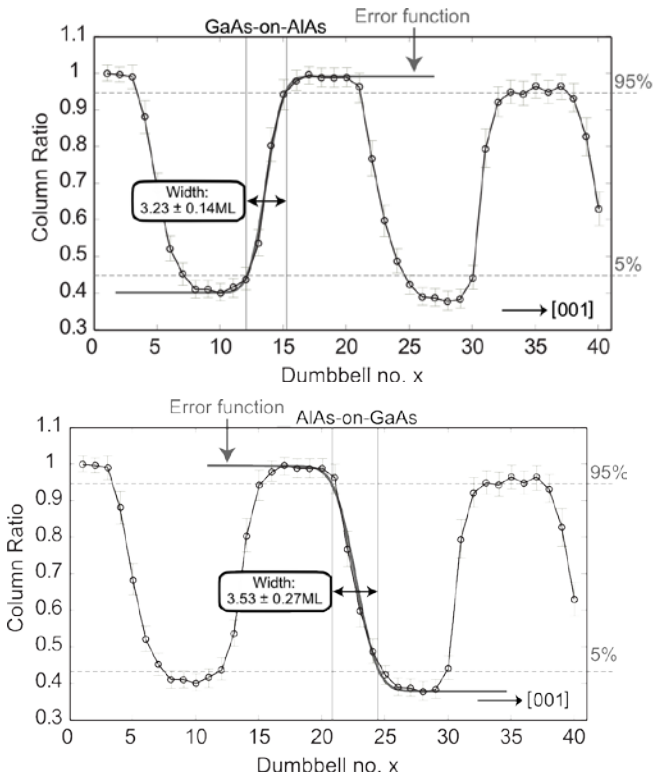

Fig. 4. (a) Column ratio profile averaged over the entire column ratio map in Fig. 3. An error function was fitted to the selected GaAs-on-AlAs interface. The interface width was measured to be equal to 3.23 ± 0.21ML from the 5% and 95% limits of the error function. (b) The error function fitted to the neighbouring AlAs-on-GaAs interface.

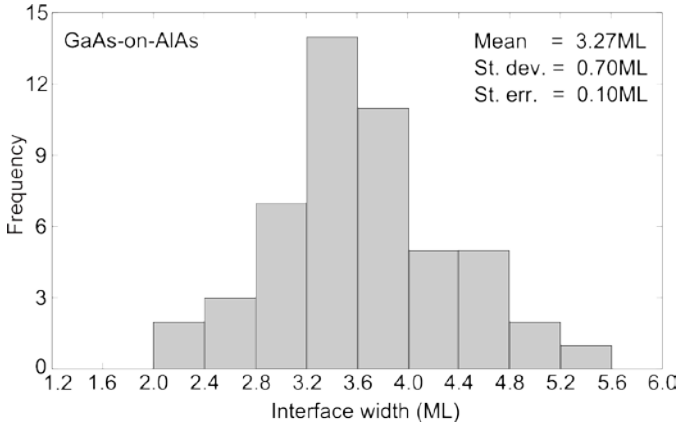

Fig. 5. Histogram of interface widths measured from the column ratio map in Fig. 3 for GaAs-on-AlAs interfaces. The mean, standard deviation and standard error are also given.

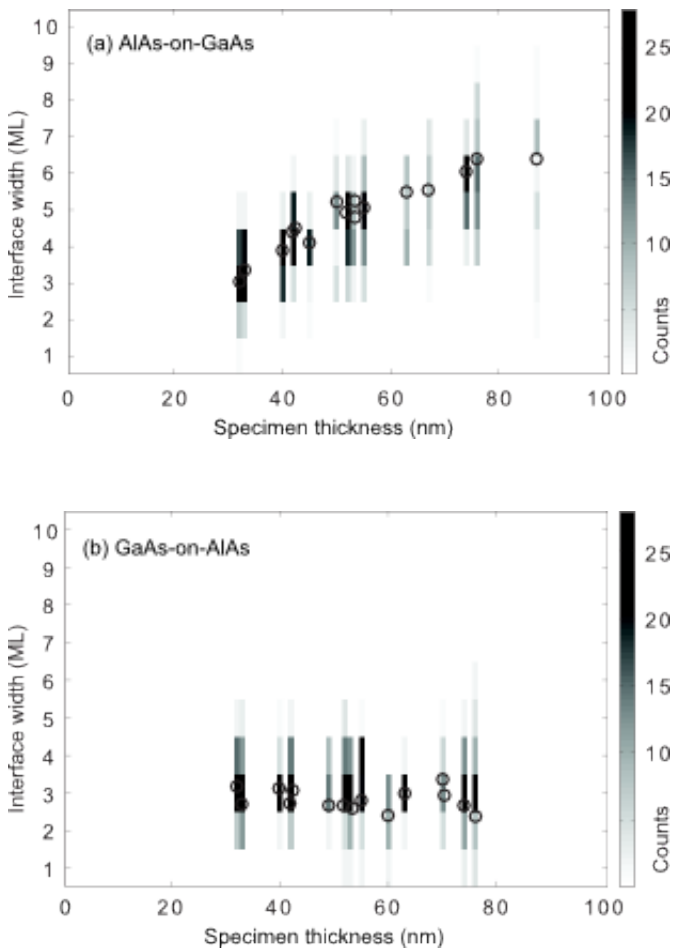

Fig. 6. The variation of interface width as a function of specimen thickness for (a) AlAs-on-GaAs and (b) GaAs-on-AlAs interfaces using the column ratio. For each thickness, the distribution of width values is represented by the greyscale-coded vertical stripes. Also shown are the average interface width values (open circles).

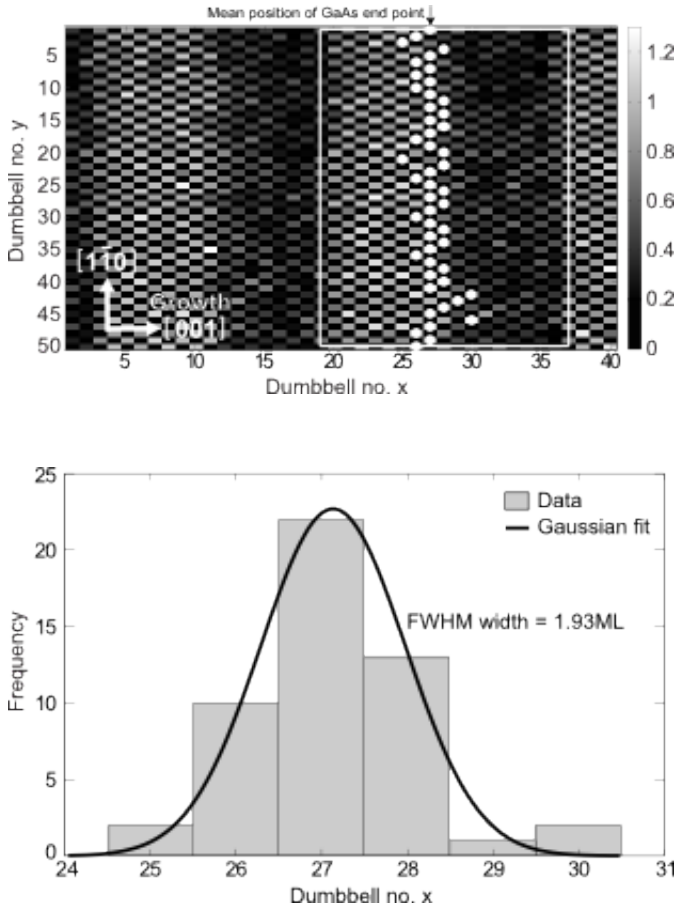

Fig. 7. (a) Column ratio map of the 9ML AlAs / 9ML GaAs superlattice at a specimen thickness of ~55nm. An 18ML wide region around a AlAs-on-GaAs interface is highlighted (box). The position of the last GaAs-like dumbbell along each horizontal row is denoted by a small circle. (b) Histogram of the last GaAs-like dumbbell positions highlighted in (a). The FWHM of the fitted Gaussian gives a measure of the sharpness in the $[1\bar{1}0]$ direction.

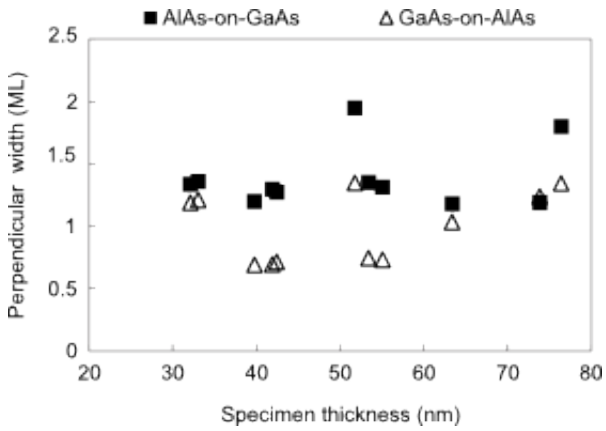

Fig. 8. The variation of the width in the $[1\bar{1}0]$ direction as a function of specimen thickness for AlAs-on-GaAs and GaAs-on-AlAs interfaces. Only data from the 9ML AlAs / 9ML GaAs superlattice is shown.

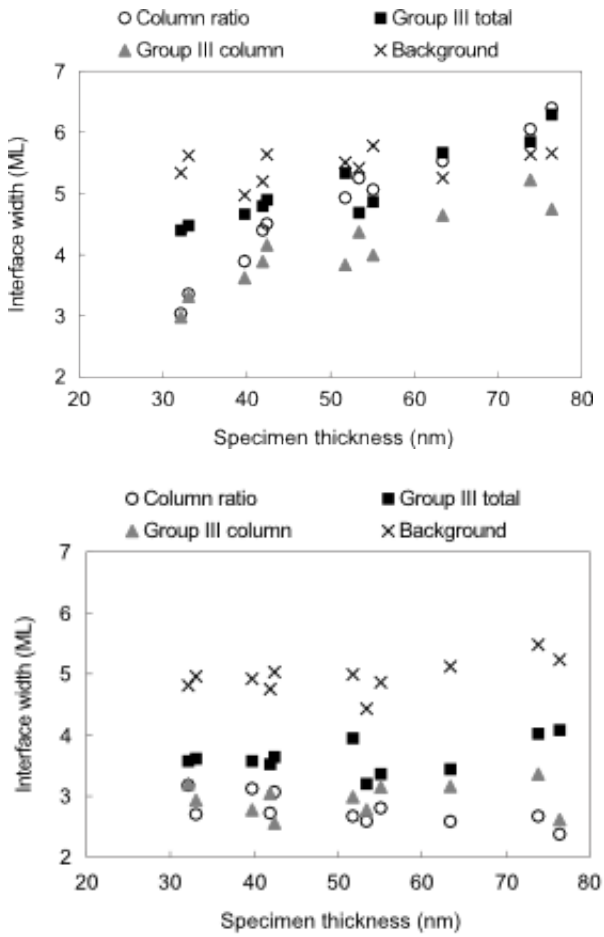

Fig. 9. The variation of interface width as a function of specimen thickness for (a) AlAs-on-GaAs and (b) GaAs-on-AlAs superlattice interfaces using the column ratio, Group III total, Group III column and background signals.

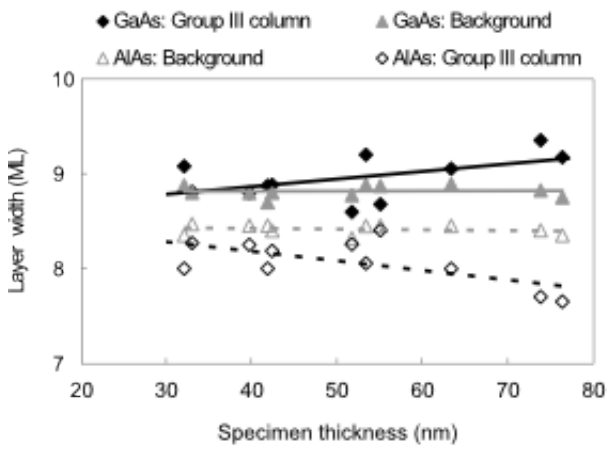

Fig. 10. The variation of layer width as a function of specimen thickness for AlAs and GaAs layers in the superlattice. The Group III column and background signals were used to measure the layer widths.